UNLIMITED DISTRIBUTION

National Defence
Research and Development Branch

Défense nationale
Bureau de recherche et développement

TECHNICAL MEMORANDUM 86/225
December 1986

WHIPPING RESPONSE OF SHIP HULLS FROM UNDERWATER EXPLOSION BUBBLE LOADING

Thomas A. Vernon

Defence Research Establishment Atlantic

Centre de Recherches pour la Défense Atlantique

Canada

DEFENCE RESEARCH ESTABLISHMENT ATLANTIC

9 GROVE STREET
P.O. BOX 1012
DARTMOUTH, N.S.
B2Y 3Z7

TELEPHONE
(902) 426-3100

CENTRE DE RECHERCHES POUR LA DÉFENSE ATLANTIQUE

9 GROVE STREET
C.P. 1012
DARTMOUTH, N.É.
B2Y 3Z7

UNLIMITED DISTRIBUTION

National Defence
Research and
Development Branch

Défense nationale
Bureau de recherche
et développement

WHIPPING RESPONSE OF SHIP HULLS FROM UNDERWATER EXPLOSION BUBBLE LOADING

Thomas A. Vernon

December 1986

Approved by B.F. Peters A/Director/Technology Division

DISTRIBUTION APPROVED BY

A/D/TD

TECHNICAL MEMORANDUM 86/225

Defence
Research
Establishment
Atlantic

Centre de
Recherches pour la
Défense
Atlantique

Canada

Abstract

A summary of the bubble pulsation dynamics of an underwater explosion is presented with the aim of establishing the whipping response of a nearby surface ship. The effects of the initial shock front are not considered and the fluid is assumed to be an incompressible medium. The gas bubble volume dynamics can then be related to far field fluid accelerations assuming that a potential flow condition is satisfied. Given the effective mass of the ship comprising the added fluid and bouyancy mass contributions, the forces on the ship resulting from the accelerated flow field can be determined. The theory considers the effects of proximity of the explosion bubble to a free surface, vertical migration of the bubble due to the hydrostatic imbalance, and an energy dissipative mechanism introduced via a pseudo pressure drag coefficient. The theory is applied in analyses of the whipping displacements and stresses induced in the hull of a typical frigate-size warship subjected to underwater blast loading. The response is obtained using a modal superposition of the wet hull modes of a detailed equivalent beam model of the hull.

Résumé

On résume la dynamique des oscillations de la bulle produite par une explosion sous-marine en vue d'établir les caractéristiques de fouettement vertical d'un navire voguant non loin en surface. On ne tient pas compte des effets du front de choc initial et on suppose que le fluide est incompressible. On peut ensuite établir un lien entre la dynamique du volume de la bulle de gaz et les accélérations du fluide dans le champ lointain si on suppose qu'une condition de champ de potentiel est satisfaite. Etant donné la masse effective du navire, y comprise les apports de la masse de fluide ajoutée et de la masse de fluide déplacée, on peut déterminer les forces exercées sur le navire par le champ d'écoulement accéléré. La théorie tient compte des effets de la proximité entre la bulle et une surface libre, de la migration verticale de la bulle à cause du déséquilibre hydrostatique et d'un mécanisme de dissipation de l'énergie représenté par un pseudo-coefficient de traînée de pression. La théorie est appliquée à des analyses des mouvements de fouettement vertical et des contraintes induits dans la coque d'un bâtiment de guerre type de la taille d'une frégate par une explosion sous-marine. La réponse est obtenue à l'aide d'une superposition modale des modes humides d'un modèle équivalent de la coque ou cette dernière est représentée en détail par une poutre.

Contents

List of Figures

Notation

a	bubble radius
$\dot{a}$	time derivative of bubble radius
A	projected area
C_d	drag coefficient
d	depth of charge
e_1, e_2	source and dipole strength coefficients
E_0	total energy of explosion
F_p	frequency of first bubble pulse
g	acceleration of gravity
k	non-dimensional energy parameter
k_1	adiabatic constant
K_{sf}	keel shock factor
L	length scale factor
P	general point in the fluid domain
r	radial distance from bubble center
t	time
T	time scale factor
T_p	period of first bubble pulse
u	fluid velocity
U	kinetic energy of bubble pulse
v	volume of bubble
V	potential energy of bubble
w	weight function

W	charge mass
x	non-dimensional bubble radius
x_0, x_m	minimum and maximum bubble radii
z	pressure head
z_0	initial pressure head
α	migration control coefficient
β	free surface effect control coefficient
γ	adiabatic gas constant
δ	non-dimensional depth
ϵ	energy/mass ($2.051 * 10^6$ joules/gm TNT)
ς	non-dimensional pressure head
ς_0	non-dimensional initial pressure head
θ	general angle
λ	non-dimensional time derivative of z $(\dot{\varsigma})$
ν	vertical bubble velocity
ρ	density of fluid
ρ_g	density of gas
σ	non-dimensional time derivative of x $(\dot{x})$
τ	non-dimensional time
ϕ	velocity potential
χ	period ratio function

1 Introduction

An underwater explosion interacts with the surrounding fluid in two different phases which are potentially damaging to a nearby ship or submarine. The first phase is a transient shock front which causes a rapid rise in the fluid velocity, and large inertial loading. This phase imparts little momentum to the fluid because of its extremely short duration. The second phase in the explosion is a radial pulsation of the gas bubble with a duration much longer than the shock phase. The pulsations are a result of the imbalance of internal explosion product pressure and the fluid hydrostatic pressure. Depending on the depth and size of the charge, several pulsations are possible, although the assumptions and theory presented in this report are considered valid for only the first complete pulse.

The bubble pulsations lead to quite significant pressure impulses on a nearby ship hull. As well as causing local damage, they tend to excite the ship in heave and natural vertical vibration modes. Because the pulsation periods are often close to the two and three-noded bending vibration frequencies of a typical frigate-size warship, a near resonant condition can exist with the potential to cause large amplitude whipping displacements. These displacements in turn can overstress the hull and, in severe cases, lead to an overall hull failure. The factors determining the whipping response of a particular ship to an underwater blast load thus depend on the characteristics of the charge as well as the vibration characteristics of the ship.

Explosion bubble dynamics have been treated by several authors[1,2,3,4], and the application of the theory in the analysis of ship whipping has been discussed extensively by Hicks[5]. The latter work, although covering many aspects of the complete problem, lacks detail and consistency in the derivation of the bubble dynamics and solution procedures required in the application of the theory. Several authors have reviewed the work as presented by Hicks and others[6,7], and have clarified certain aspects of the theory; however, the derivation and solution of the bubble dynamical equations has remained somewhat confusing. In this report, the bubble energy equations are summarized clearly in a manner intended to facilitate a numerical solution procedure. The assumptions are explicitly stated for the various cases treated, and a solution procedure is discussed. The algebraic development is not given in detail, and the interested reader is referred to References 2, 5 and 6 for further discussion.

The presentation of the bubble dynamic equations begins with the simplest case of a non-migrating bubble far from the free surface. In this and all subsequent derivations, a potential flow regime is assumed to be valid. For this first case, the single differential equation describing the bubble radius can be effectively integrated with Tschebycheff polynomials. The introduction of bubble migration and free surface effects result in a system of first order differential equations which can be integrated via a Runge-Kutta algorithm. A drag term analogous to that for a solid body wake can be introduced in the bubble migration

equation to account for energy dissipation during the bubble expansion and contraction. This term has little theoretical justification, but provides an adjustment parameter to give energy dissipation rates in agreement with experimental results.

The solution of the bubble expansion and migration equations provides an analytical description of the velocity potential. The far field fluid velocities, accelerations, and pressures can then be obtained from application of the appropriate operators on the velocity potential in accordance with potential flow theory and general fluid dynamics. The fluid accelerations, which are used in the current approach, define a time-dependent forcing function per unit mass at a point in the far field. This function can be spatially averaged and scaled by the appropriate mass term to provide a point load force time history representing the effective load on a hull segment. The response of the ship can then be determined via direct integration methods or, more commonly, by modal superposition.

Because of the simplicity and accepted accuracy of equivalent beam representations of ships in the evaluation of low frequency vibrations, such models are often used in the prediction of whipping response to underwater explosions. Typically, a minimum of twenty sections are used to represent both the hydrodynamic form and structural characteristics of the ship. A recent study indicates that this is an acceptable level of discretization for the determination of the lowest modes of vibration of a frigate hull.[8] In the present study, one hundred sections are used for the structural representation of a test ship typical of a modern frigate. Twenty sections are used for the hydrodynamic description. The hydrodynamic coefficients of form can be used with the traditional Lewis form methods[9] to obtain the mode-dependent sectional added fluid masses associated with hull vibration. Alternative methods of obtaining added masses independent of the vibration mode are also available, and are applied in the determination of the wet modes of the hull in the current study. Once the added mass terms are known, an eigenvalue analysis of the beam model including this mass will provide with sufficient accuracy the first 3 or 4 vertical bending modes of the hull. These modes in turn define a suitable basis for solution of the forced equations of motion via modal superposition.

Section 2 of this report presents the derivations of the bubble equations, and Section 3 discusses the application of the theory in the analysis of the response of the test ship to underwater blast loads using the methods outlined in the text. A final section includes some concluding remarks on the reliabilty of the theory and general comments on the results of the analysis.

2 Bubble Dynamics

A number of assumptions are implicit in the derivation of the bubble pulsation and migration equations, and the prediction of the response of nearby bodies to the bubble

dynamics. First, as discussed above, the compressible phase of the explosion is neglected completely on the basis that the impulse of that phase is very small compared to the pressure impulses of the bubble pulsations. Secondly, the fluid is considered incompressible and irrotational, and a potential flow regime is assumed to represent the fluid motion caused by the expansion and contraction of the bubble. Thirdly, the bubble shape is assumed to remain spherical throughout the pulsations. This is an adequate approximation for the expansion phase although large distortions tend to occur near the end of the contraction phase. These deviations from the spherical shape make this assumption a poor one for the analysis of subsequent bubble pulses. Finally, a far field approximation is made in the derivations in this report whereby the ship is assumed to have no influence on the bubble dynamics. The effects of close proximity and contact explosions can be treated;[5] however, in that case local damage rather than whipping is the primary concern.

Several cases are treated in order of complexity beginning with the simple case of a non-migrating bubble in deep water. In all cases an energy conservation approach is used to derive the pulsation dynamics, and the losses due to acoustic radiation and cooling of the gas products are neglected. This last point is very important since it essentially limits the accuracy of this form of derivation to single bubble pulses. The energy dissipative mechanisms which control the inter-bubble phase are not well understood, and approximations are all that is possible in this approach.

2.1 Deep bubble approximation

At significant depth and hence large ambient pressure, an underwater explosion bubble is not affected by the free surface reflection, and undergoes little vertical migration because of the low bouyancy forces associated with a reduced bubble radius. The bubble center can be considered as a stationary, singular source with a time dependent strength. The fluid velocity potential resulting from the source becomes,

$$\phi = \frac{e_1}{r} \tag{1}$$

The time dependent source strength parameter, e_1, can be determined by considering the fluid velocity at the surface of the bubble. The bubble volume time rate of change is,

$$\dot{v} = 4\pi r^2 \dot{r} = 4\pi r^2 \frac{\partial \phi}{\partial r} \tag{2}$$

hence,

$$e_1 = -\frac{\dot{v}}{4\pi} \tag{3}$$

and,

$$\phi = \frac{\dot{v}}{4\pi r} \tag{4}$$

The fluid velocity at a distance r from the explosion source is then,

$$u = \frac{a^2 \dot{a}}{r^2} \tag{5}$$

An energy equation based on the conservation of total energy in the system can be formulated,

$$E_0 = U + V \tag{6}$$

where E_0 is the initial energy of the explosive, determined from the knowledge of the mass and type of charge, and U and V are the kinetic and potential energies of the explosion bubble. The kinetic energy associated with the explosion bubble is the energy of the surrounding fluid, given by the integral,

$$U = \frac{1}{2} \int_a^\infty \rho u^2 (4\pi r^2)\, dr \tag{7}$$

The potential energy is the sum of the pressure potential of the explosion void and the internal energy of the gas products. The complete energy equation can be expressed in terms of the bubble radius, a, and its derivatives as,[1]

$$E_0 = 2\pi\rho a^3 \dot{a}^2 + \frac{4}{3}\pi\rho a^3 g z_0 + \frac{k_1}{(\gamma - 1)} \frac{(W)^\gamma 3^{\gamma-1}}{(4\pi)^{\gamma-1} a^{3(\gamma-1)}} \tag{8}$$

where an adiabatic equation of state has been assumed valid for the explosion reaction. This equation can be written in the much simpler form,

$$x^3 \dot{x}^2 + \frac{k}{x^{3(\gamma-1)}} + x^3 - 1 = 0 \tag{9}$$

by introducing the non-dimensional factors,

$$x = \frac{a}{L} \tag{10}$$

$$\tau = \frac{t}{T} \tag{11}$$

with,

$$L = \left[\frac{3E_0}{4\pi\rho g z_0}\right]^{\frac{1}{3}} \tag{12}$$

$$T = \left[\frac{3}{2g z_0}\right]^{\frac{1}{2}} \tag{13}$$

$$k = \frac{(\rho g z_0)^{\gamma-1}}{\gamma - 1} k_1 \left(\frac{W}{E_0}\right)^\gamma \tag{14}$$

Based on experimental evidence,[10] it is necessary that $\gamma = \frac{5}{4}$ if equation (9) is to describe the behaviour of the bubble. For the theoretical and experimental bubble half periods, T, to agree, the following relation is specified,

$$E_0 = \epsilon W \tag{15}$$

with ϵ as the energy/unit mass given as approximately $2.051 * 10^6$ joules/gram for TNT. Comparisons of peak pressures indicate that,

$$k \simeq 0.0743(z_0)^{\frac{1}{4}} \tag{16}$$

for units of meters, kilograms and seconds. Hence the specification of the charge type, mass and depth allows the calculation of the time and length scale factors, and it remains to find the solution $x(\tau)$, given by equation (9). This equation can be written as,

$$\frac{dx}{\sqrt{x^{-3} - kx^{-3\gamma} - 1}} = dt \tag{17}$$

Integrating,

$$\tau = \int_{x(\tau=0)}^{x(\tau)} \frac{dx}{\sqrt{x^{-3} - kx^{-3\gamma} - 1}} \tag{18}$$

This integral can be evaluated very effectively using Tschebycheff polynomials,[11] where the integral I defined as,

$$I = \int_a^b \frac{f(y)}{\sqrt{(y-a)(b-y)}}\ dy \tag{19}$$

can be integrated as,

$$I = \sum_{i=1}^{n} w_i f(y_i) + R_n \tag{20}$$

where R_n is a small remainder term. For the integrals of interest in the present study, near exact integration is obtained using an eight term expansion ($n = 8$). The function is evaluated at,

$$y_i = \frac{(b+a)}{2} + \frac{(b-a)}{2} x_i \tag{21}$$

with,

$$x_i = \cos \frac{(2i-1)}{2n} \pi \tag{22}$$

and the weight function is in this case a constant,

$$w_i = \frac{\pi}{n} \tag{23}$$

Using this approach, the bubble radius time function is rewritten as,

$$\tau = \int_{x_0}^{x_m} \frac{\sqrt{(x-a)(b-x)}}{\sqrt{x^{-3} - kx^{-3\gamma} - 1}}\, dx \tag{24}$$

It is evident that the evaluation of this integral provides the time at which the radius assumes a particular value, as opposed to a more common time integration process. The integrand causes problems when the denominator function goes to zero. This occurs at the minimum and maximum radii of the bubble, x_0 and x_m respectively, and these values must become the integration limits to avoid singularities in the integral. These points can be determined from the roots of the denominator function, which is equivalent to setting $\dot{x} = 0$ in equation (9). In fact, the roots of this expression are quite sensitive to the value of k, which reflects the dependence of the bubble dynamics on the energy of the bubble and the ambient pressure. In comparisons with small scale experiments from which the theory is calibrated,[2,5] the magnitude of k remains small, (of order 0.1 - 0.2). In such cases, this approach works well even for multiple pulses; however, for realistic depths of discharge in the ship whipping context, the k value is initially quite low, but increases rapidly beyond a 'small' value when energy losses are introduced in attempts to apply the theory to multiple bubble pulses. In many cases, no positive roots of the function will exist for other than the first pulse, and the method cannot predict multiple pulse behaviour. If reasonably small energy attenuations are assumed, multiple pulses can be predicted by the theory.

The description of energy attenuation, which is critical in the application of this approach for prediction of multiple bubble pulses, is not well defined. Classical literature suggests losses of approximately 70 percent of the initial energy for the second pulse, and a further 50 percent reduction for the third pulse. Implementation of these values in the above derivation leads to only one bubble pulse for realistic charge depths. Other energy attenuations might be used, since results of small scale experiments indicated reasonably constant reductions of roughly 60 percent for each pulse. These latter reductions are used to obtain the results presented in Section 3.

2.2 Effects of migration

The vertical migration of the gas bubble can be included very simply in the definition of the velocity potential function. In this case, Figure 2, the potential function is given as,

$$\phi = \frac{e_1}{r} + \frac{e_2}{r^2}\cos\theta \tag{25}$$

The strength coefficients can be evaluated on the bubble surface to give,

$$e_1 = \frac{\dot{v}}{4\pi} = a^2\dot{a} \tag{26}$$

$$e_2 = \frac{a^3\nu}{2} \tag{27}$$

where ν is the mean vertical bubble velocity. Applying the conservation of energy procedure as in the first case, the energy equation becomes,

$$E_0 = \pi\rho a^3(2\dot{a}^2 + \frac{1}{3}\nu^2 + \frac{4}{3}gz) + \frac{k_1}{(\gamma-1)}\frac{(W)^\gamma 3^{(\gamma-1)}}{(4\pi)^{\gamma-1}a^{3(\gamma-1)}} \tag{28}$$

The first term corresponds to the kinetic energy of the fluid, the second term the kinetic energy of migration, the third the gravitational potential, and the fourth term the pressure potential of the explosion products. This expression can be non-dimensionalized to give the bubble equation of motion in the form,

$$\frac{d}{d\tau}(x^3\dot{x}^2 + x^3\dot{\varsigma}^2 + x^3\frac{\varsigma}{\varsigma_0} + \frac{k}{x^{3(\gamma-1)}}) = 0 \tag{29}$$

where ς_0 is the initial non-dimensionalized total head at discharge depth, and ς is the non-dimensionalized head as a function of time. An application of Lagrange's equation to the energy expressions,

$$\frac{d}{dt}(\frac{\partial}{\partial\dot{z}}(U-V) = \frac{\partial}{\partial z}(U-V) \tag{30}$$

gives the equation of motion governing the migration of the bubble as,

$$\frac{d}{d\tau}(x^3\dot{\varsigma}) = -\frac{3x^3}{\varsigma_0} \tag{31}$$

Differentiating, we can form a system of first order equation suitable for integration with a standard Runge-Kutta integration algorithm,

$$\sigma = \dot{x} \tag{32}$$

$$\lambda = \dot{\varsigma} \tag{33}$$

$$\dot{\sigma} = -\frac{3}{2}\left(\frac{\sigma^2}{x} - \frac{\lambda^2}{6x} + \frac{\varsigma}{x\varsigma_0} - \frac{(\gamma-1)k}{x^{3\gamma+1}}\right) \tag{34}$$

$$\dot{\lambda} = -3\left(\frac{1}{\delta_0} + \frac{\sigma\lambda}{x}\right) \tag{35}$$

The initial conditions for the solution of this system are taken as,

$$x = x_0 \tag{36}$$

$$\varsigma = \varsigma_0 \tag{37}$$

$$\sigma = 0 \tag{38}$$

$$\lambda = 0 \tag{39}$$

where x_0 is taken as the minimum root of the radius function discussed in the case of the non-migrating bubble. The solution of these equations defines the velocity potential function, which in turn will provide the far field fluid pressures and accelerations. The derivation of the fluid accelerations is discussed in the final case of this section.

2.3 Free surface effects

Neglecting the existence of gravity waves, the free surface is defined as a contour of zero potential. This can be satisfied by defining the surface as a plane of anti-symmetry, and placing a negative image bubble above the plane. The effect of this image is a cancelation of the horizontal pressure gradient and accelerations at the free surface, and a doubling of the vertical components. This can be done very simply as the last stage of the solution procedure. Such an approach implies that the free surface has no effect on the bubble dynamics, which is true for reasonably deep charges; however, where the bubble pulse is within several radii of the free surface, the presence of the surface reflection does influence the motion of the bubble, and the dynamical equations must be modified. In this case, the velocity potential is reformulated as,

$$\phi = \frac{e_1}{r} + \frac{e_2}{r^2}\cos\theta - \frac{e_1}{r_1} + \frac{e_2}{r_1}\cos\theta_1 \tag{40}$$

Enforcing the bubble surface velocities, the strength coefficients are found to be,

$$e_1 = a^2\dot{a} \tag{41}$$

$$e_2 = \frac{a^3}{2}\left(\nu - \frac{a^2\dot{a}}{4d^2}\right) \tag{42}$$

where d is the depth of the bubble center below the free surface, Figure 3. In fact, typical of imaging methods, an infinite number of images are required to balance the higher order terms introduced into the expression for the velocity potential, and the use of only a single image is an approximation. Neglecting terms of order higher than $(\frac{a}{d})^2$, the energy conservation equation becomes,

$$E_0 = \pi\rho a^3\left[2\dot{a}^2(1-\frac{a}{2d}) + \frac{1}{3}\dot{a}\nu(\frac{a^2}{d^2}) + \frac{4}{3}gz\right] + \left(\frac{4\pi a^3}{3}\right)^{(\gamma-1)}\frac{k_1(W)^\gamma}{\gamma-1} \tag{43}$$

Non-dimensionalizing, we obtain,

$$\frac{d}{d\tau}\left[x^3(\dot{x}^2(1-\frac{x}{2\delta}) + \frac{1}{6}\dot{\varsigma}^2 + \frac{1}{4}\dot{x}\dot{\varsigma}(\frac{x}{\delta})^2 + \frac{\varsigma}{\varsigma_0}) + \frac{k}{x^{3(\gamma-1)}}\right] = 0 \tag{44}$$

where $\delta = \frac{d}{L}$. Again using the Lagrange equation, the bubble migration equation becomes,

$$\frac{d}{d\tau}\left[\frac{x^3\dot{\varsigma}}{3}\right] = -\left[\frac{3x^4\dot{x}^2}{4\delta^2} + \frac{x^5\dot{x}^2}{4\delta^2} + \frac{x^3}{\varsigma_0}\right] \tag{45}$$

Taking the derivatives, a system of first order equations can be formed similar to those of equations (32)-(35), and the same initial conditions can be used.

2.4 Bubble drag forces

Experimental results have shown that the migration velocities predicted by the theory outlined above are too large. To control these velocities, a pseudo drag coefficient is introduced and the energy dissipation of that force is included in the overall energy conservation equation. This drag term is not particularily realistic, since drag coefficients reflect the interaction of a solid body and the surrounding fluid, whereas the explosion bubble is a surface of constant pressure. However, the controllable energy dissipation of the drag force allows a better correlation of theoretical and experimental results. The drag force is defined in the conventional manner,

$$F = \frac{1}{2}\rho C_d A \nu^2 \tag{46}$$

where A is the projected area of the bubble, in this case a circle of radius a. Although the projected area of the bubble is largest at its maximum radius, the largest drag forces and energy dissipation occur near the bubble minimum radius. This is a result of the much higher migration velocities which are imparted to the bubble due to the momentum in the fluid acting on a body with a much decreased added fluid mass. Inclusion of the drag force in the energy conservation equation leads to the bubble expansion equation as,

$$\frac{d}{d\tau}\left[x^3(\dot{x}^2(1-\frac{x}{2\delta}) + \frac{\dot{\varsigma}^2}{6} + \frac{1}{4}\dot{x}\dot{\varsigma}(\frac{x}{\delta^2}) + \frac{\varsigma}{\varsigma_0}) + \frac{k}{x^{3(\gamma-1)}}\right] = C_d\frac{x^2\dot{\varsigma}^3}{4} \tag{47}$$

and the migration equation,

$$\frac{d}{d\tau}\left[\frac{x^3\dot{\varsigma}}{3}\right] = -\left[\frac{3x^4\dot{x}^2}{4\delta^2} + \frac{x^5\ddot{x}}{4\delta^2} + \frac{x^3}{\varsigma_0}\right] + C_d\frac{x^2\dot{\varsigma}^2}{4} \tag{48}$$

Performing the differentiation, we obtain the system of equations,

$$\dot{x} = \sigma \tag{49}$$

$$\dot{\varsigma} = \lambda \tag{50}$$

$$\dot{\sigma} = -\frac{3\delta}{(2\delta - \beta x)}\left[\frac{\sigma^2}{x}(1 - \frac{2\beta x}{3\delta}) - \frac{\lambda^2}{6x} + \frac{\varsigma}{x\varsigma_0} - \frac{(\gamma-1)k}{x^{3\gamma+1}} + \frac{\beta x}{4\delta^2}(C_d\frac{\lambda^2}{4x} + \frac{\sigma\lambda}{3} - \frac{x}{\varsigma_0})\right] \quad (51)$$

$$\dot{\lambda} = -3\alpha\left[\frac{1}{\varsigma_0} + \frac{\sigma\lambda}{x} - C_d\frac{\lambda^2}{4x} + \frac{\beta x}{4\delta^2}(3\sigma^2 + x\dot{\sigma})\right] \quad (52)$$

The α and β are convenient programming controls which can be set to a value of one if the effects of migration and the free surface respectively are to be included. The equations can then be programmed in one subroutine for use in all cases in which the initial conditions of equations (36)-(39) are utilized.

A drag coefficient can be determined by matching the energy dissipation and migration predictions to experimental results, and a value of approximately 2.0 - 2.5 appears to give reasonable agreement. This is well in excess of normal drag coefficients for solid bodies, hence either the assumption of spherical shape is not realistic, or the drag theory does not apply to moving pressure surfaces. Regardless of its theoretical basis, the drag mechanism can be used for correlation purposes.

The strength coefficients of the velocity potential of equation (40) can be expressed in terms of the scale factors and non-dimensional functions as,

$$e_1 = \frac{L^3x^2}{T}\sigma \quad (53)$$

$$e_2 = \frac{L^4}{2T}(x^3\lambda - \frac{x^5\sigma}{4\delta^2}) \quad (54)$$

The time derivatives of these coefficients required in the derivation of the fluid accelerations are then given as,

$$\dot{e_1} = \frac{L^3}{T^2}(2x\sigma^2 + x^2\dot{\sigma}) \quad (55)$$

$$\dot{e_2} = \frac{3L^4\sigma x^2}{2T^2}\left[\lambda - \frac{x^2\sigma}{4\delta^2}\right] + \frac{x^3L^4}{2T^2}\left[\dot{\lambda} - (\frac{2x\sigma + x^2\dot{\sigma}}{4\delta^2})\right] \quad (56)$$

2.5 Fluid accelerations

Once the fluid velocity function is defined, the fluid velocities and accelerations in the far field can be calculated. For potential flow, the velocity is the negative gradient of the potential,

$$u_y = -\bigtriangledown\phi = -\frac{\partial\phi}{\partial y} \quad (57)$$

In cartesian coordinates, Figure 2, this gives,

$$u_y = \frac{1}{(x^2+y^2)}\left[\frac{e_1y}{(x^2+y^2)^{\frac{1}{2}}} - \frac{e_2}{(x^2+y^2)^{\frac{1}{2}}}(1 - \frac{3y^2}{(x^2+y^2)})\right] \quad (58)$$

From the general theory of fluid dynamics, the fluid accelerations are given as,

$$\dot{u}_y = \frac{\partial u}{\partial t} - \nu \frac{\partial u}{\partial y} \tag{59}$$

The two terms of this expression can be evaluated to give,

$$\frac{\partial u}{\partial t} = \frac{1}{(x^2+y^2)^{\frac{3}{2}}} \left[\dot{e_1} y - \dot{e_2}(1 - \frac{3y^2}{(x^2+y^2)}) \right] \tag{60}$$

$$\frac{\partial u}{\partial y} = \frac{e_1}{(x^2+y^2)^{\frac{3}{2}}}(1 - \frac{3y^2}{(x^2+y^2)}) + \frac{3ye_2}{(x^2+y^2)^{\frac{5}{2}}}(3 - \frac{5y^2}{(x^2+y^2)}) \tag{61}$$

These expressions can be substituted into equation (59) to obtain the far field fluid accelerations. Once the accelerations are known, the forces can be calculated by averaging the accelerations over segments of the ship hull, and scaling by the effective mass of the section. The mass term will include the bouyancy mass of the hull, and the added fluid mass associated with vertical vibration of the hull. These terms can be found by various methods, and are assumed to exist in the formulation given in this report.

2.6 Solution outline

Based on the previous development, the generation of a load time history for an explosion can be summarized in the following steps:

1. Establish initial conditions and scale factors of the bubble pulse from the specified depth, charge mass and energy conversion factor (Equations (9)-(14)).

2. Begin integration of the relevant equations from the initial conditions. The integration time step should be some appropriately small fraction of the overall period of the pulse.

3. At each time step, calculate $e_1, e_2, \dot{e_1}, \dot{e_2}$, the fluid acceleration $\dot{u}_y$ and the force $m\dot{u}_y$ (Equations (53)-(56) and (59)).

4. Finish integration at a predetermined cut-off time. This can be estimated from the time scale factor. If migration is included, the integration is terminated when the bubble surface contacts the free surface.

5. If multiple pulses are possible, apply the energy dissipation criterion at the bubble minimum radii, and repeat steps 1-4 above.

The above approach has been adopted in the coding of a short, interactive computer program, UBLOAD. This program accesses the equivalent beam properties data file created by SCRAP[12] to obtain the sectional fluid masses. The sectional masses are used in conjunction with the hull form coefficient data file to calculate the effective mass of the ship. Utilizing user-specified information on the charge depth, standoff, and mass, the program calculates the time history of the bubble motion with either the Tchebycheff polynomial (for the deep bubble approximation only) or Runge-Kutta integration method. A sample program run with explanatory comments is included in the Appendix. The far field fluid accelerations and force time history are calculated for all nodes available in the structural representation of the ship. This data is stored in a format suitable for direct use in the finite element program VAST.[13]

3 Predictions from the theory

The characteristics of two underwater explosions are presented to illustrate the results of the methods discussed in Section 2. The charge characteristics have been taken such that comparisons with results available in the literature[5,6] can be made. Very close agreement with the available literature has been obtained for these bubble characteristic time histories.

The first blast corresponds to a small, shallow charge with a mass of 45.5 Kg. of TNT at a depth of 7.6 m. Figure 4 presents the first pulse radius time history for the various assumptions available in the method. In this case, the non-migrating results are derived from the Tchebycheff method, which appears to give a pulse period which is too low in comparison to that obtained using the Runge-Kutta methods, Figure 5. The discrepancy appears to be a result of the time step and symmetrizing algorithm used in the Tchebycheff approach. Although that method could be improved, it is simpler to use the Runge-Kutta method for all cases, and this has been done in all further tests.

The bubble radius, depth, velocity, and pressure radius time histories for the shallow charge are presented in Figures 5,6,7 and 8 respectively. The results for the migrating bubble stop when the bubble surface reaches the fluid surface, hence these are more realistic than those from the non-migrating assumption, which predicts multiple pulsations. It is evident that the maximum bubble radius is not sensitive to the various assumptions; however, the bubble period changes significantly. The effect of the free surface is to decrease the bubble period. Figure 7 indicates the phenomenon associated with the fluid momentum lag which causes large peaks in the bubble velocity time history at the time of the minimum radius. These peaks are largest when the effects of the free surface are included.

The pressure radius and maximum fluid acceleration time histories of Figures 8 and 9 indicate that the neglect of bubble migration will lead to the prediction of erroneously large pressure and acceleration peaks and multiple pulses. The error caused by the neglect of migration is not as serious as would appear from consideration of only maximum values, since the response of a body is dependent primarily on the impulse of the forcing function rather than simply the magnitude of the quite transient peaks. The variation in the impulses predicted for the three assumptions is in fact fairly low; however, the prediction of multiple pulses in this case is not an acceptable result.

The second blast modelled with the theory is a large, deep charge of 227 Kg, at a depth of 45.7 m. The time history characteristics of this charge are presented in Figures 10 - 14. The theory predicts two complete pulses before the radius function becomes singular. The effect of the energy dissipation factor between the pulses is evident in the lower bubble maximum radius of the second pulse. In this case, neither the bubble radius or period are particularily sensitive to the assumptions of migration, indicating that the deep bubble approximation would be reasonably accurate for this range of depth.

3.1 Bubble pulse frequency specification

Based on a combination of physical intuition and previously obtained results, a worst case whipping scenario for a ship subjected to a blast load will result when the following conditions are met:

1. The charge is directly under the ship (no standoff).

2. The charge is approximately amidships.

3. The bubble pulse frequency and first natural hull bending frequency are matched.

4. There are multiple pulses.

The first two criteria can easily be satisfied by defining the appropriate charge location. It is not as evident how the latter two conditions can be fulfilled; however, several relationships can be exploited to obtain the charge characteristics which result in a specific bubble pulse period. From equations (12),(13) and (15), the time scale parameter T is found to be related to the charge mass and pressure head at the charge depth by the relation,

$$T = 1.428 \frac{W^{\frac{1}{3}}}{z_0^{\frac{5}{6}}} \tag{62}$$

for the meter, kilogram, second unit system, where,

$$z_0 = d + 10 \tag{63}$$

The keel shock factor[14] in this system is defined as,

$$K_{sf} = 2.21\frac{\sqrt{W}}{d} \tag{64}$$

Based on a series of numerical tests, the time scale parameter can be related in an approximate manner to the first bubble pulse period T_p, as shown in Figure 15. These curves have been generated from repeated analyses with migration and free surface effects included. The relationship is evidently a function of depth but is not strongly dependent on the charge mass in the range of variables appropriate in the whipping problem. This function is denoted $\chi(z)$, and has been approximated with three linear segments for the purposes of this study. We can then write,

$$T_p = \frac{T}{\chi(z)} = 1.428\frac{W^{\frac{1}{3}}}{\chi(z)(d+10)^{\frac{5}{6}}} \tag{65}$$

For a specified keel shock factor, the bubble pulse frequency then becomes,

$$F_p = \frac{\chi(z)(2.21\sqrt{W} + 10K_{sf})^{\frac{5}{6}}}{1.428\, W^{\frac{1}{3}} K_{sf}^{\frac{5}{6}}} \tag{66}$$

This equation has been used to generate the curves shown in Figure 16. The specification of a frequency then allows a charge mass to be chosen such that a specific keel shock factor will result. The charge depth for that keel shock factor can be obtained from Figure 17. The keel shock factor in this system simply provides a convenient relationship between the charge mass, depth, and explosion strength relative to the hull.

It is evident from Figure 16 that there are numerous combinations of charge depth and mass which will give a specific bubble pulse frequency. If matched to the lower frequencies representative of the primary bending modes of a frigate-sized hull, these combinations will result in high keel shock factors. In such cases, local damage as well as whipping will no doubt be important. Lower keel shock factors can be obtained if the second vertical bending and bubble pulse frequencies are matched. The selection of a particular charge mass and depth from Figures 16 and 17 does not necessarily provide multiple pulses. This is difficult to predict a priori because of the effects of migration on the bubble depth and period, and a more comprehensive numerical investigation would be required to provide some simple means of predicting the occurrence of multiple pulses. Since the theory is inherently less accurate for subsequent pulses because of the unrepresentative modelling of the energy dissipation and bubble distortion mechanisms, such an investigation is probably not justified.

3.2 Application of the Theory

It is informative and indeed the end objective to apply the whipping theory in the prediction of the response of an actual ship. To this end, a very detailed equivalent beam model of a typical frigate-size warship has been created, from which the wet hull modes could be calculated. Included in the prediction of these natural frequencies were the effects of shear area coefficients, deckhouse stiffness contribution, and consideration of the structurally ineffective material in the upper decks. The added fluid mass associated with the hull vibration modes was calculated using the line dipole method presented by Hicks.[5] The first few natural frequencies obtained from this model are presented in Table 1.

TABLE 1: Natural frequencies of the test ship (Hz.)

Mode 1[a]	Mode 2[b]	Mode 3[a]	Mode 4[c]	Mode 5[b]	Mode 6[c]
1.68	2.48	3.94	4.62	5.14	6.25

[a] Vertical bending mode
[b] Horizontal bending mode
[c] Coupled bending mode

Using Figures 16 and 17, a charge mass and depth were selected to provide a first bubble frequency of 1.68 Hz For the purposes of this example, a keel shock factor of approximately 1.2 was used. The design charts indicate that a mass of approximately 167 Kg and depth of 24 m would result in the appropriate bubble frequency. The frequency from the integrated time history was 1.66 Hz, indicating that the design method can give quite adequate results. The charge was placed directly below the keel at a point 70 m from the forward perpendicular, a position selected on the basis of a brief study of the charge position versus hull response for a constant depth and mass charge.[8] For the test ship, this charge position resulted in the largest hull displacements.

The hull response was calculated using modal superposition of the first three vertical hull modes. The acceleration time history responses of the bow and stern of the ship are presented in Figure 18. The contribution of higher modes is evident, but the overall response is controlled by the fundamental mode with period 0.58 seconds. A peak acceleration of slightly greater than 1.0 g is predicted at the bow, and a peak of approximately 0.75 g at the stern. This is consistent with the primary bending mode shape of the ship, which has larger displacements in the bow than the stern.[8] The higher modal effects are not evident in the displacement response, Figure 19, which is completely dominated by the primary bending mode. In an explosion not tuned to the primary bending mode, contributions from the second and third modes have been noted, although they are quite nominal. A maximum displacement of approximately 73 mm occurs at the bow due to this explosion.

The maximum stress induced in the hull from the whipping motions is predicted to be 70-80 MPa in the midship area. This stress level is well below the midship stresses

expected from the design wave loading[8] and the response in this case is completely elastic. The maximum pressures at the keel are not expected to cause any permanent local plate deformation for this load case.

4 Conclusion

The spherical explosion bubble theory is fairly widely used to predict the whipping response of ship hulls to underwater blast loads. The theory as presented is relatively simple, if not completely physically realistic. The inclusion of the effects of the free surface and bubble migration appear to give predictable behaviour in the bubble characteristic time histories, and simple numerical techniques can be used to calculate those time histories. The major drawback in the theory is, from the point of view of this author, its inability to accurately model the multiple pulse phenomenon; however, it is conservative to adopt the approach taken in this study, in which the charge masses, and hence bubble energies, are scaled from pulse to pulse. Unfortunately, the value of that scale factor is not well defined.

Regardless of the specific limitations of the current approach, the whipping response analysis is a global response problem, and the magnitude of hull displacements or accelerations will be little affected by minor changes in bubble characteristics. The methods adopted in the UBLOAD program are stable, efficient, and give results consistent with intuition.

The design charts developed to allow tuning of the bubble pulse and hull natural frequency can be used effectively to generate a worst case loading scenario for a given keel shock factor. The application of the method in the prediction of the whipping response of a ship is straightforward, given an equivalent beam representation of the hull, and the hydrodynamic characteristics of the hull form. The study of the frigate response to underwater blast loading has indicated the form and magnitude of the response to be expected in such a ship, and comparisons of the predicted response to the results of any large scale shock trials of this ship would be valuable.

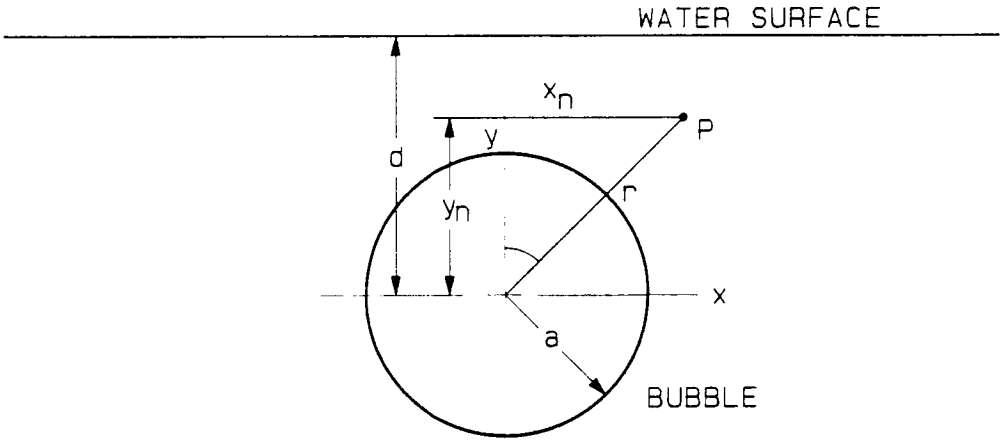

Figure 1: Geometry of explosion bubble and far field

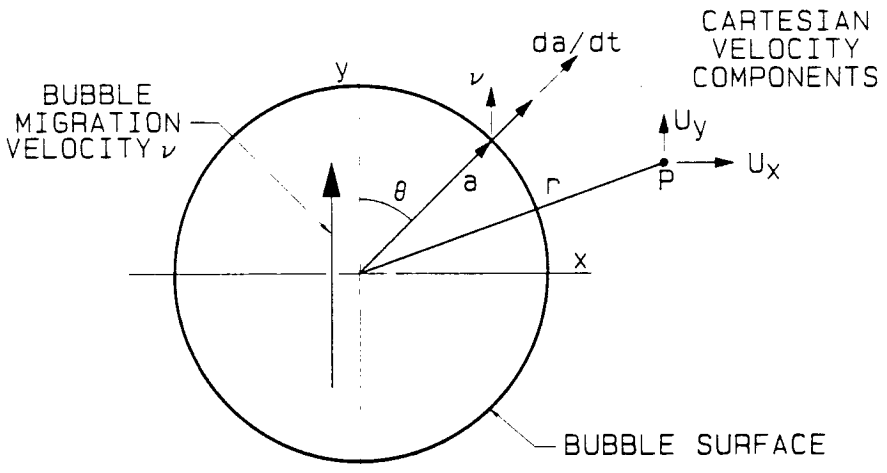

Figure 2: Geometry of migrating explosion bubble and far field velocity

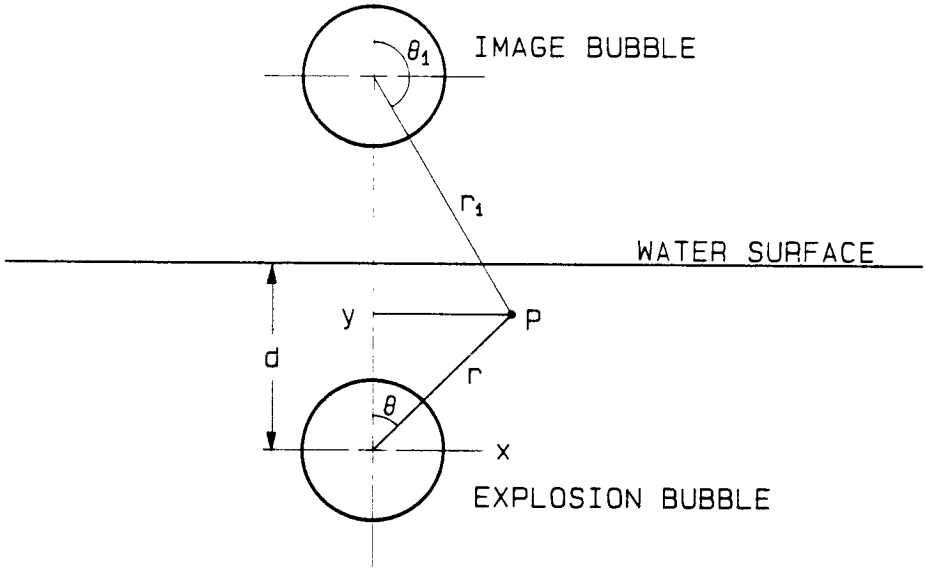

Figure 3: Image and source bubble geometry

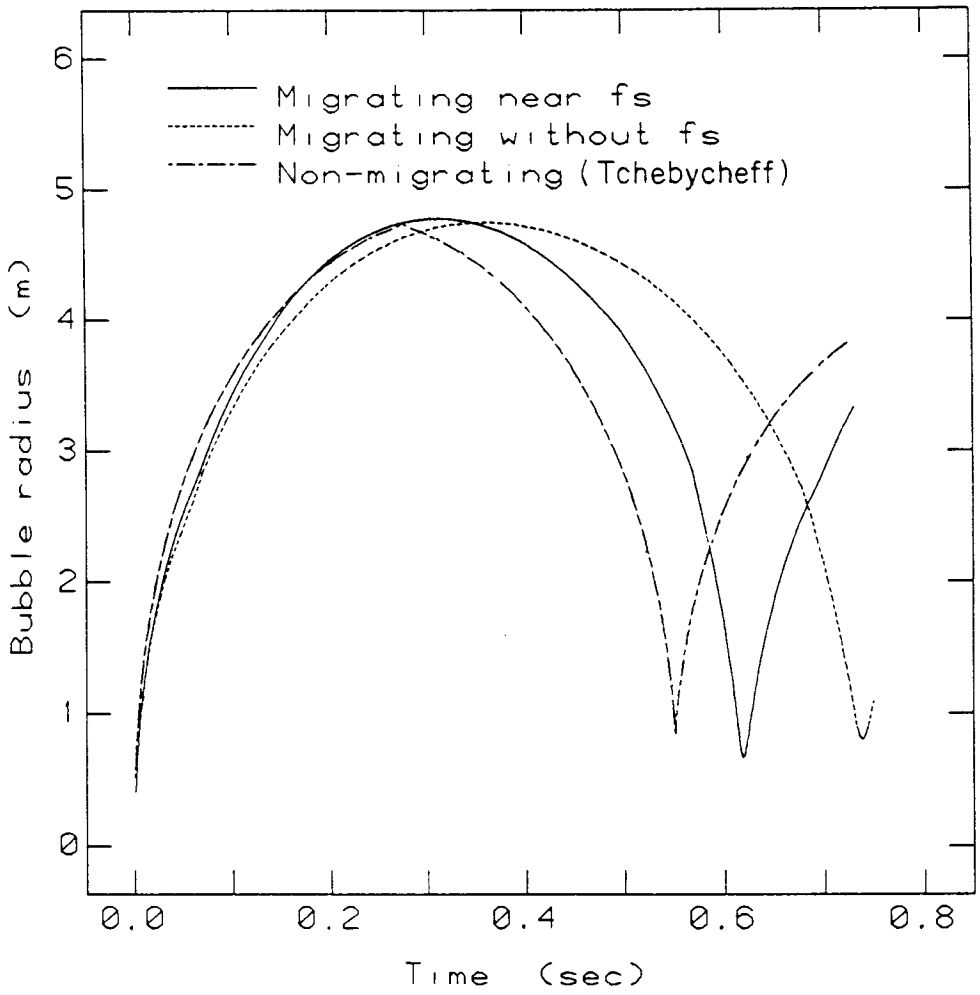

Figure 4: Bubble radius time history for the first pulse for a charge of 45.5 Kg. of TNT at a depth of 7.6m.

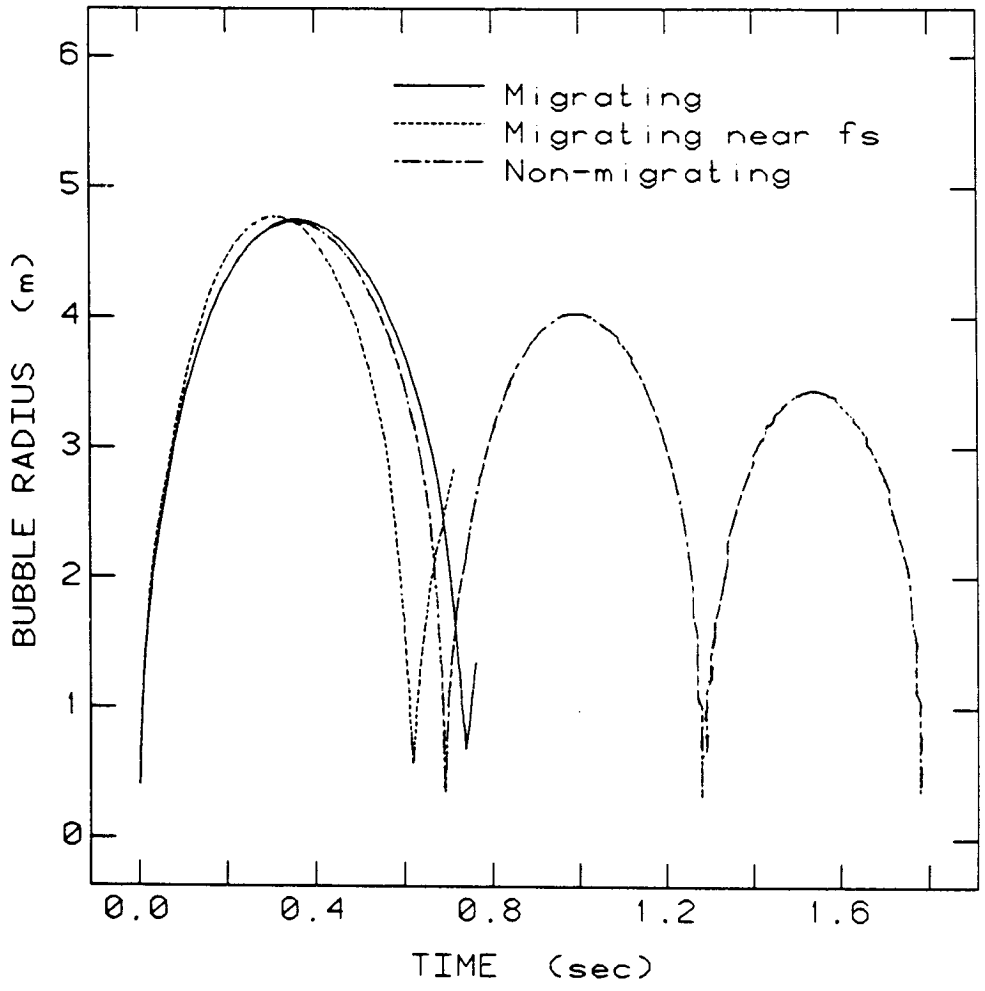

Figure 5: Bubble radius time history for a charge of 45.5 Kg. of TNT at a depth of 7.6m.

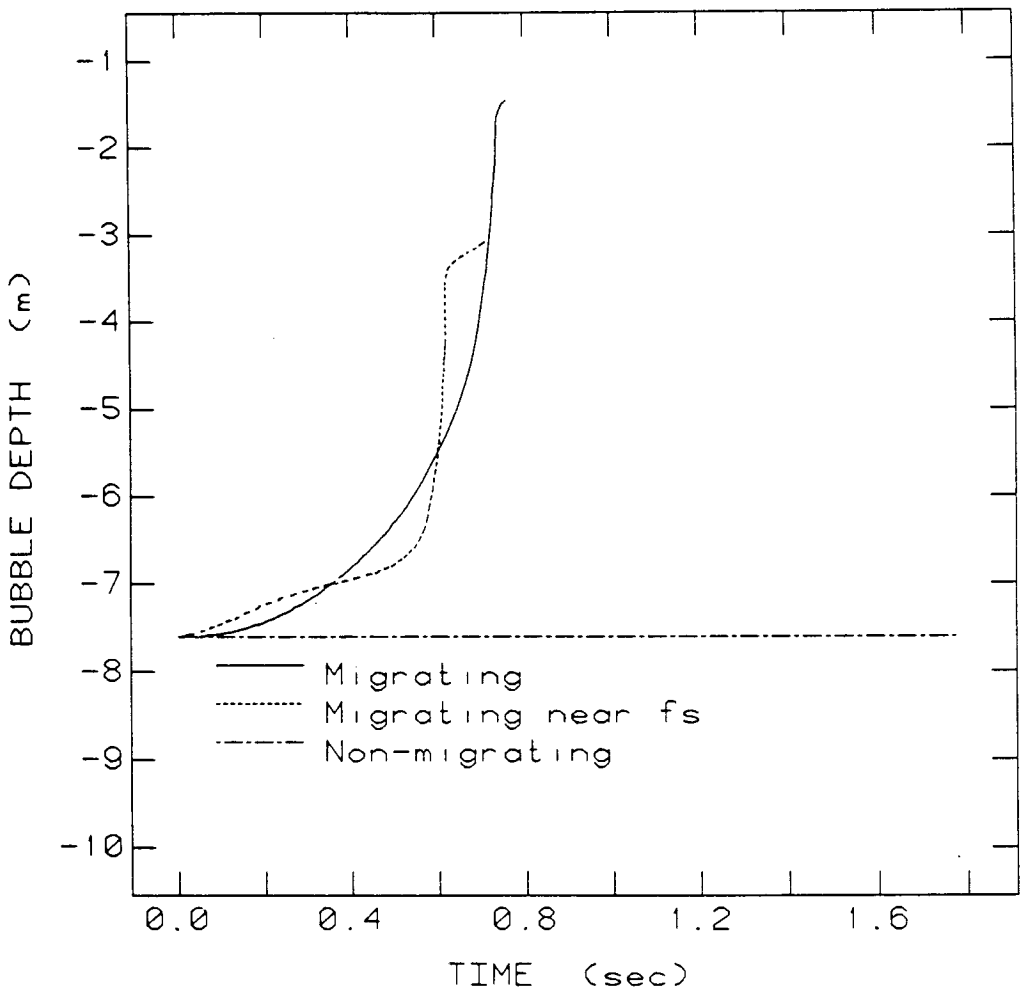

Figure 6: Bubble depth time history for a charge of 45.5 Kg. of TNT at a depth of 7.6m.

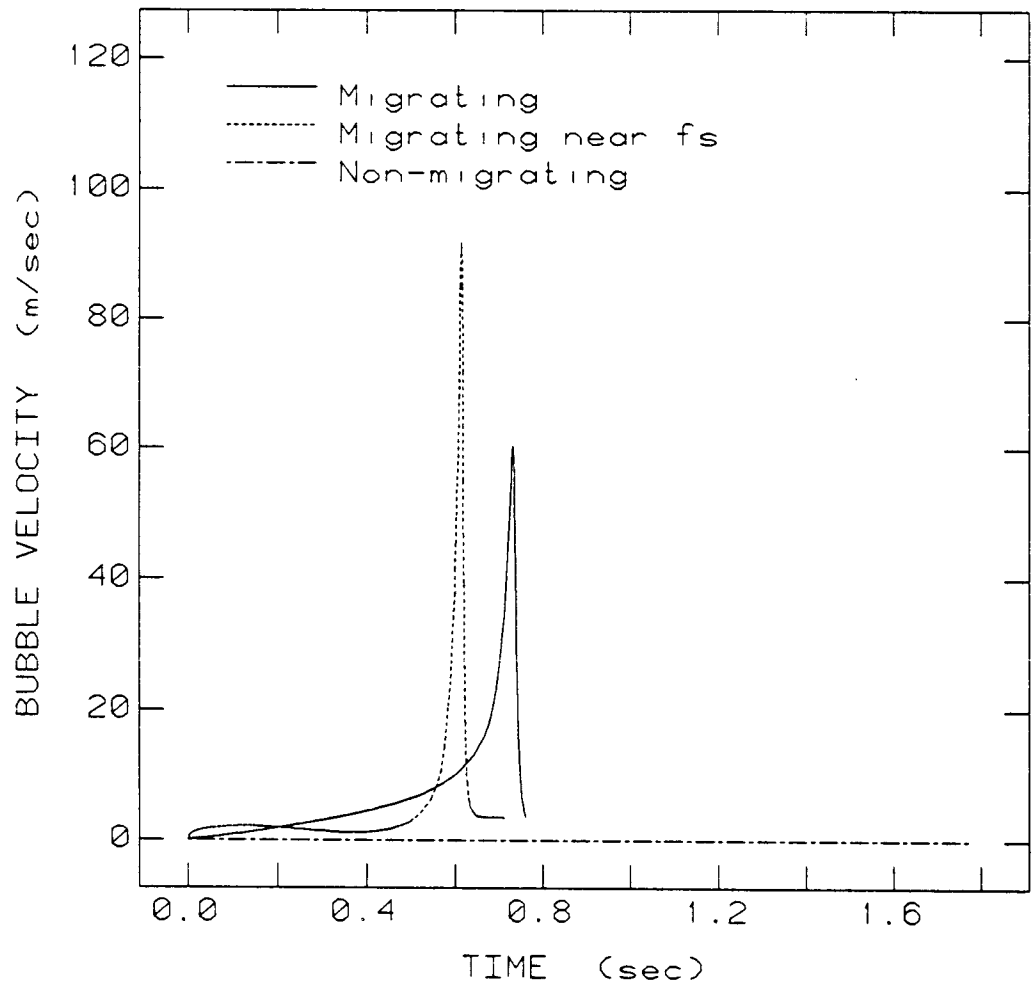

Figure 7: Bubble velocity time history for a charge of 45.5 Kg. of TNT at a depth of 7.6m.

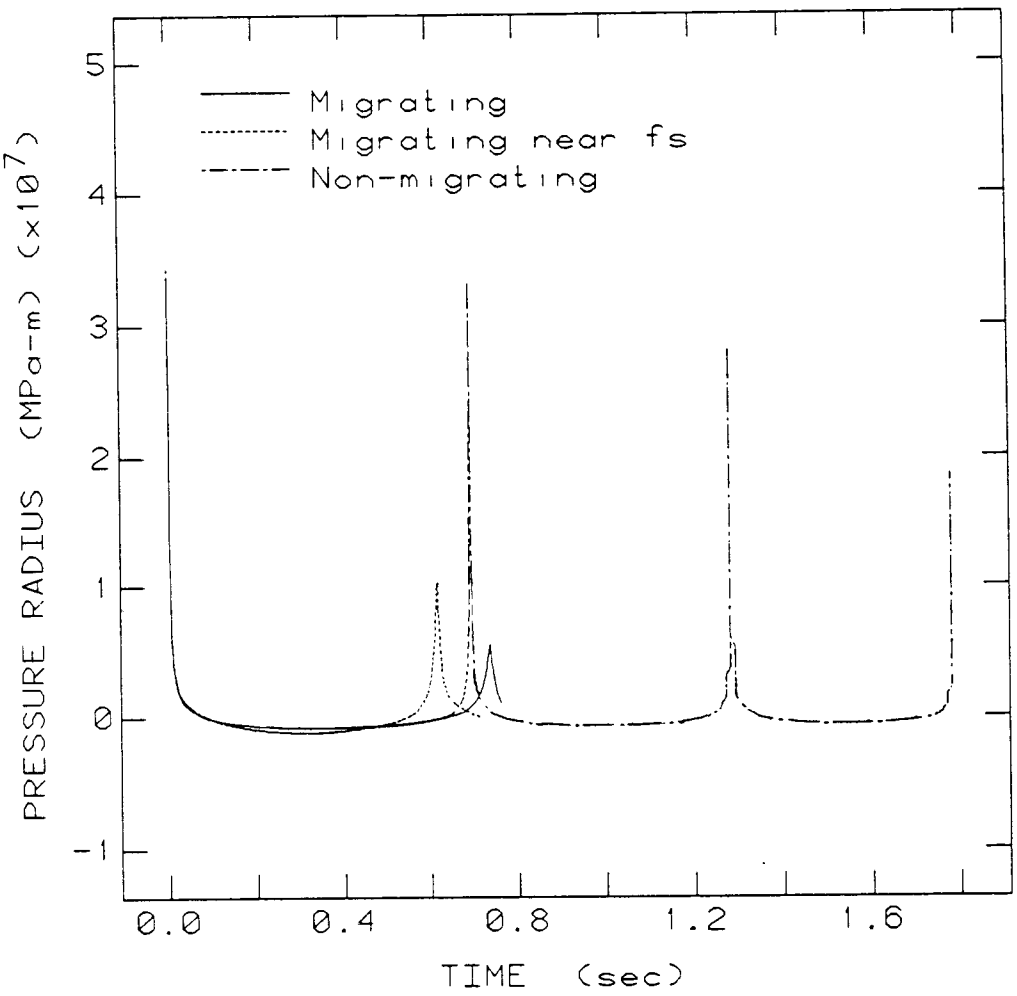

Figure 8: Pressure-radius time history for a charge of 45.5 Kg. of TNT at a depth of 7.6m.

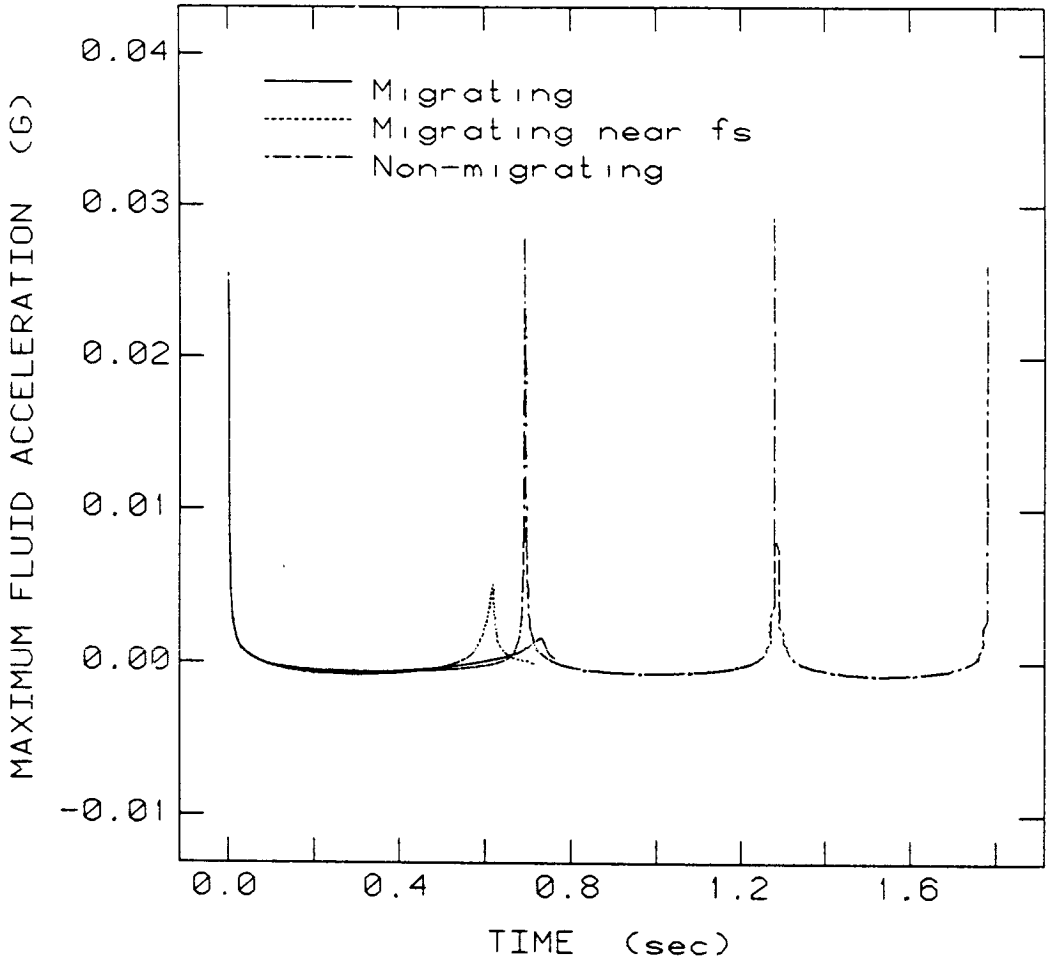

Figure 9: Maximum fluid acceleration time history for a charge of 45.5 Kg. of TNT at a depth of 7.6m.

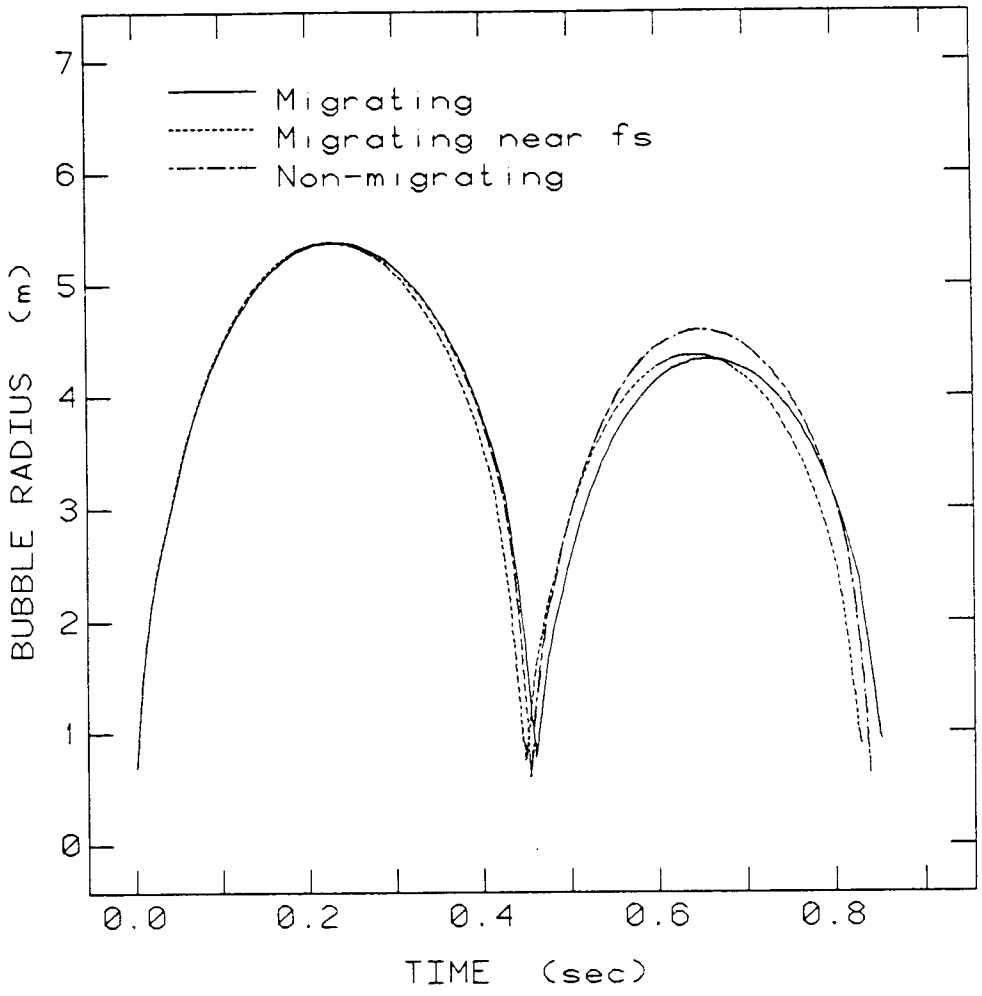

Figure 10: Bubble radius time history for a charge of 227 Kg. of TNT at a depth of 45 m.

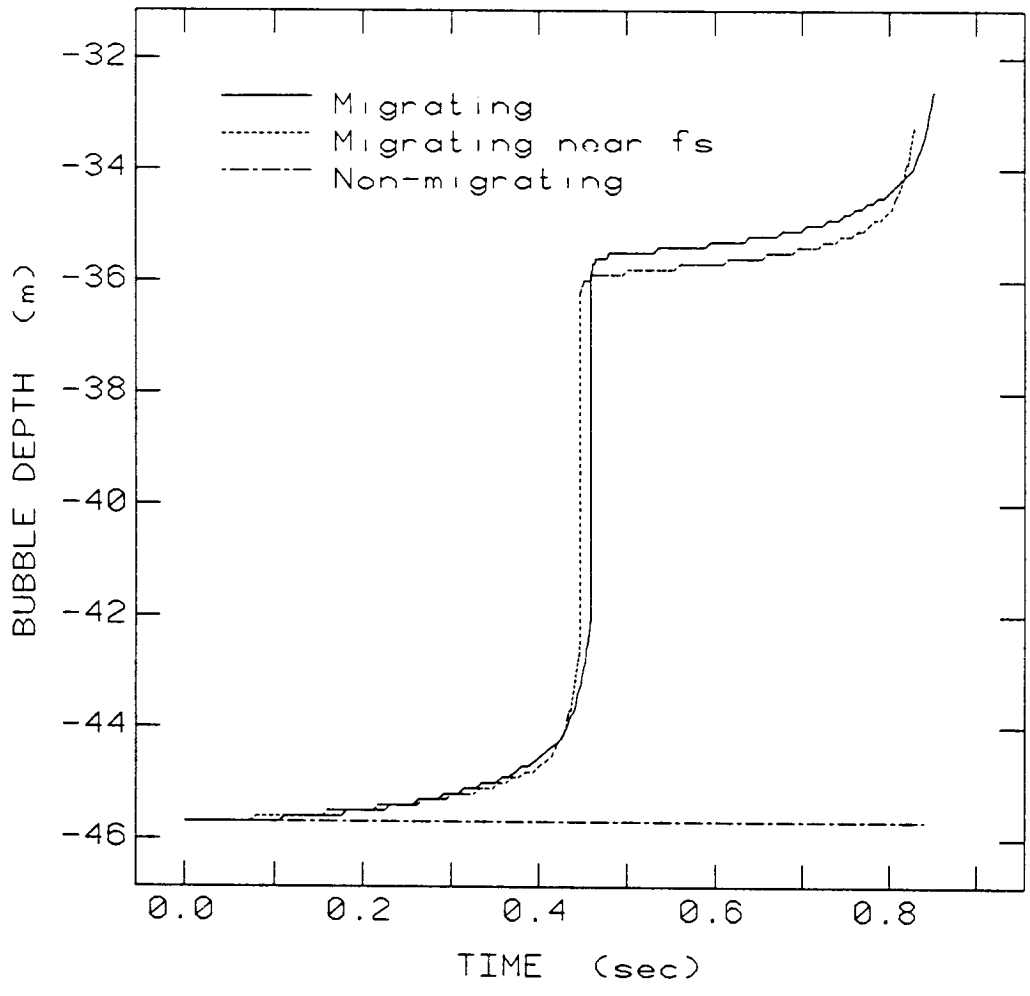

Figure 11: Bubble depth time history for a charge of 227 Kg. of TNT at a depth of 45 m.

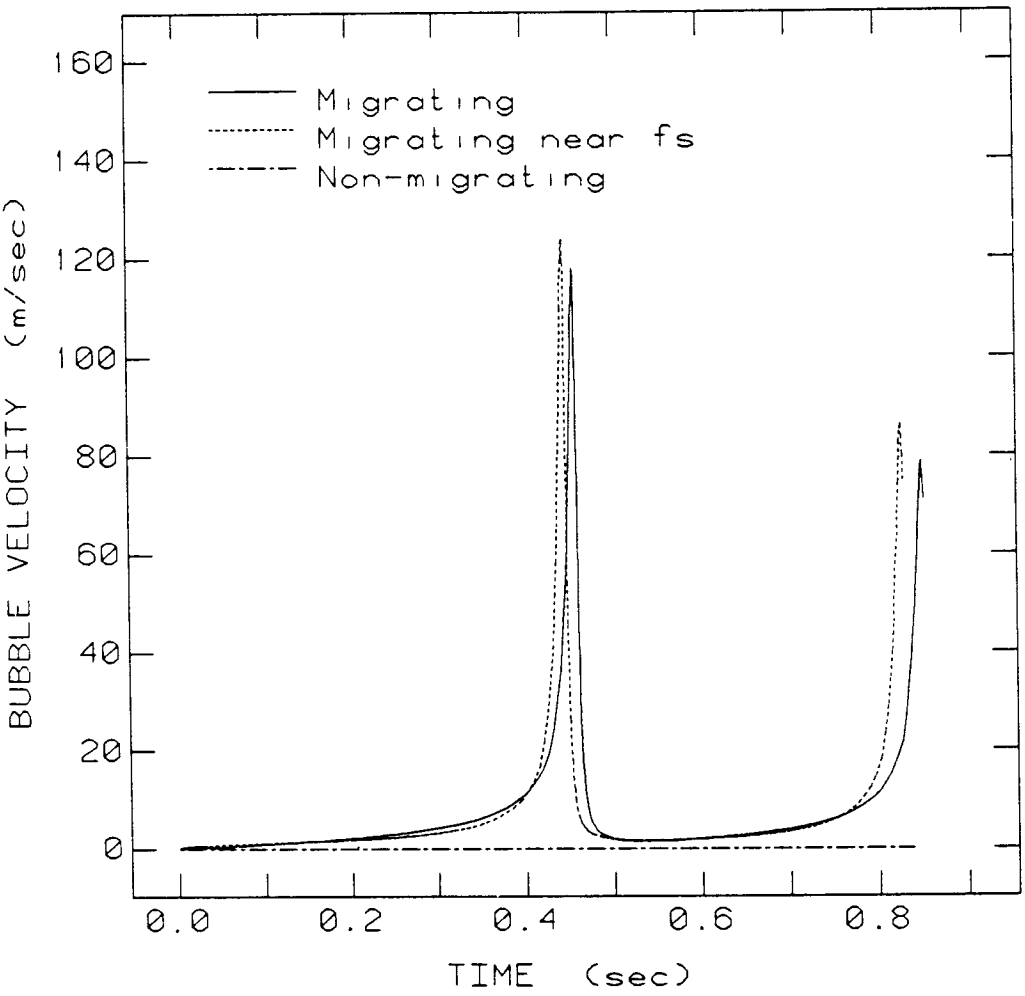

Figure 12: Bubble velocity time history for a charge of 227 Kg. of TNT at a depth of 45 m.

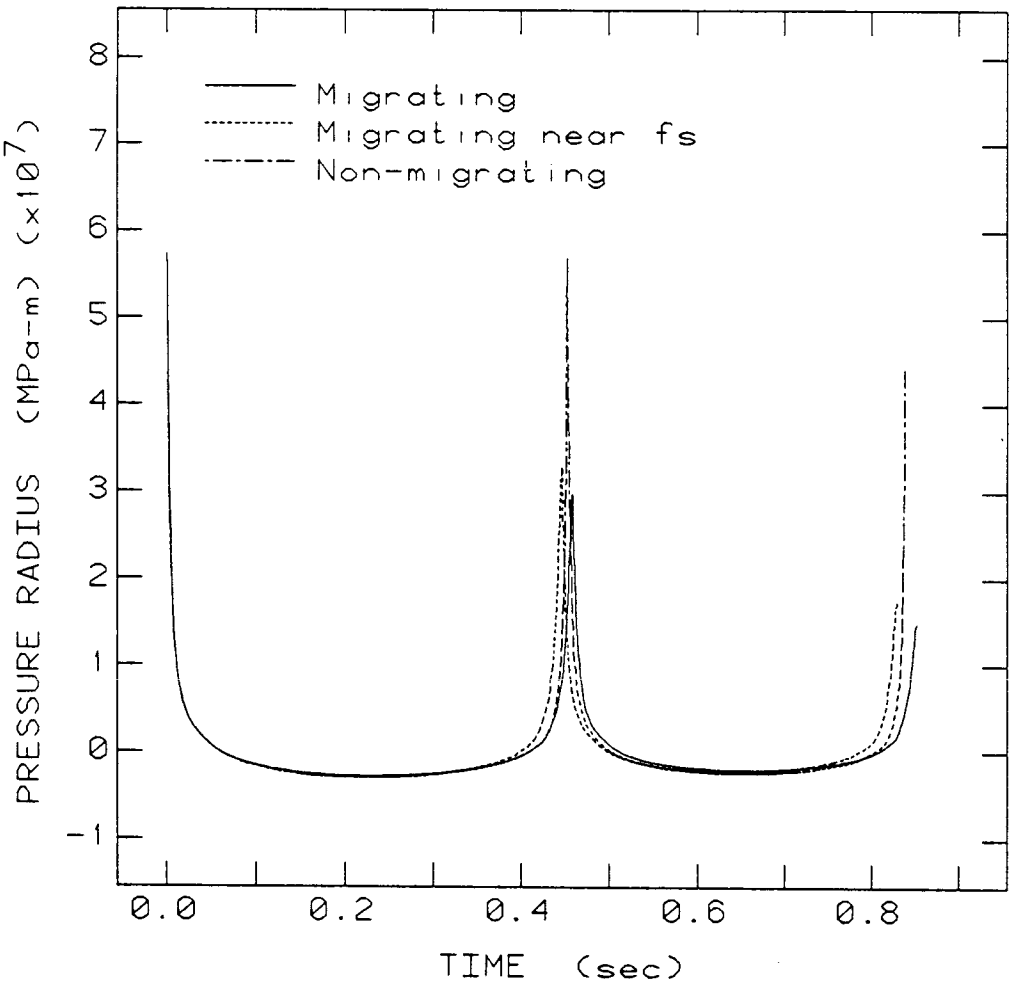

Figure 13: Pressure-radius time history for a charge of 227 Kg. of TNT at a depth of 45 m.

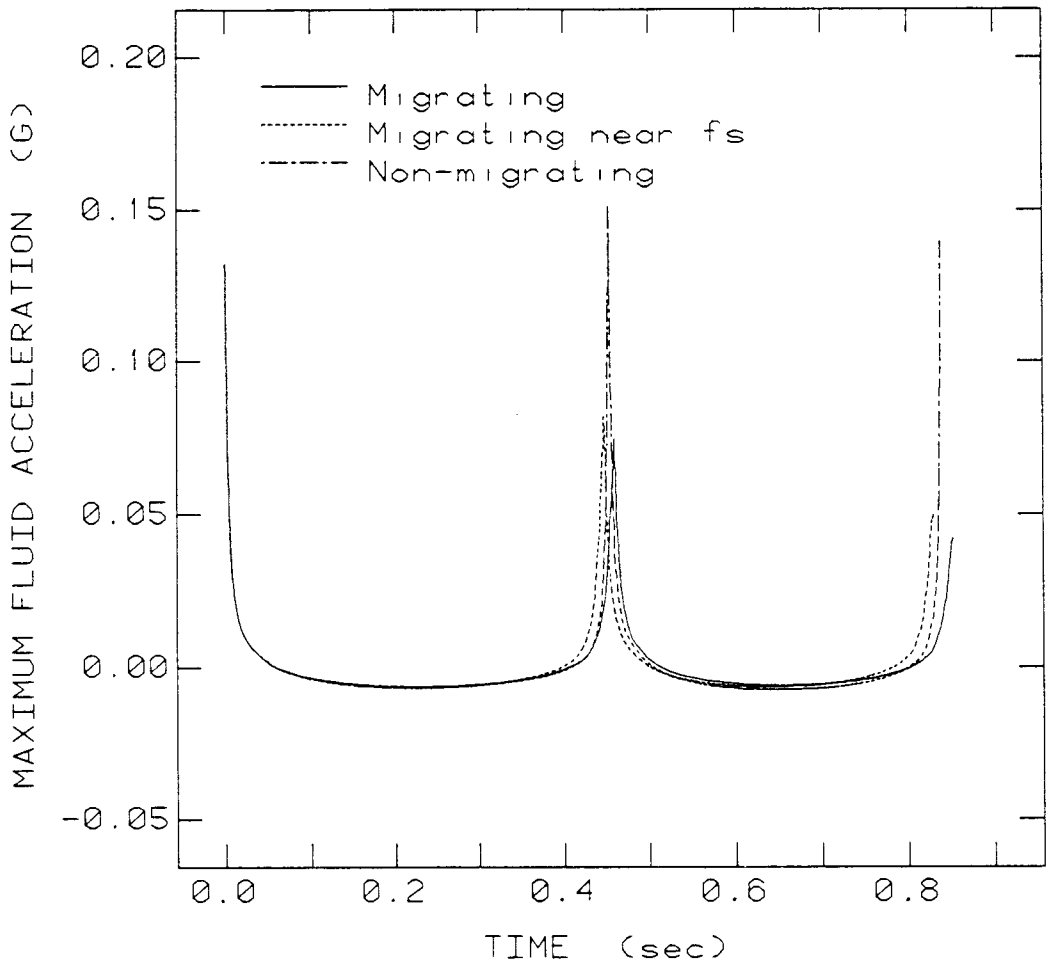

Figure 14: Maximum fluid acceleration for a charge of 227 Kg. of TNT at a depth of 45 m.

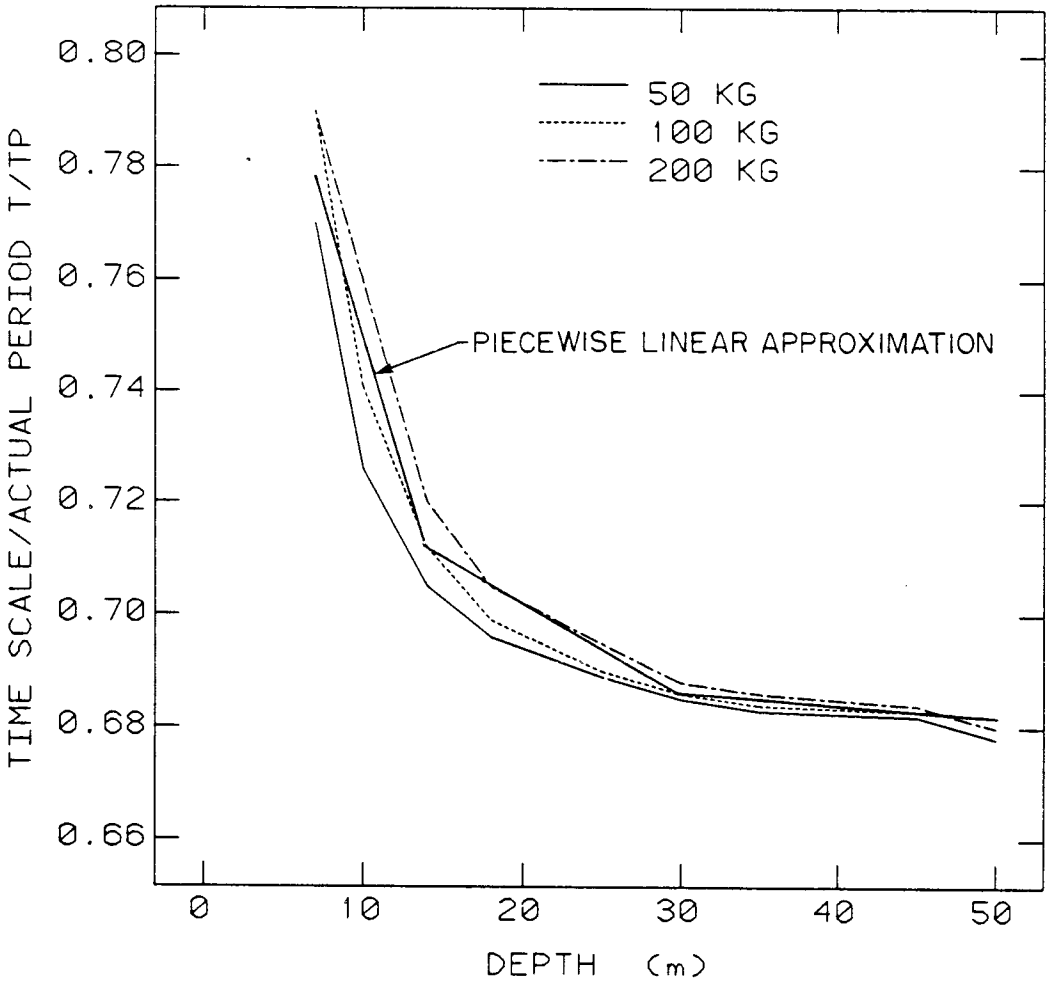

Figure 15: Period ratio as a function of depth for various charge masses.

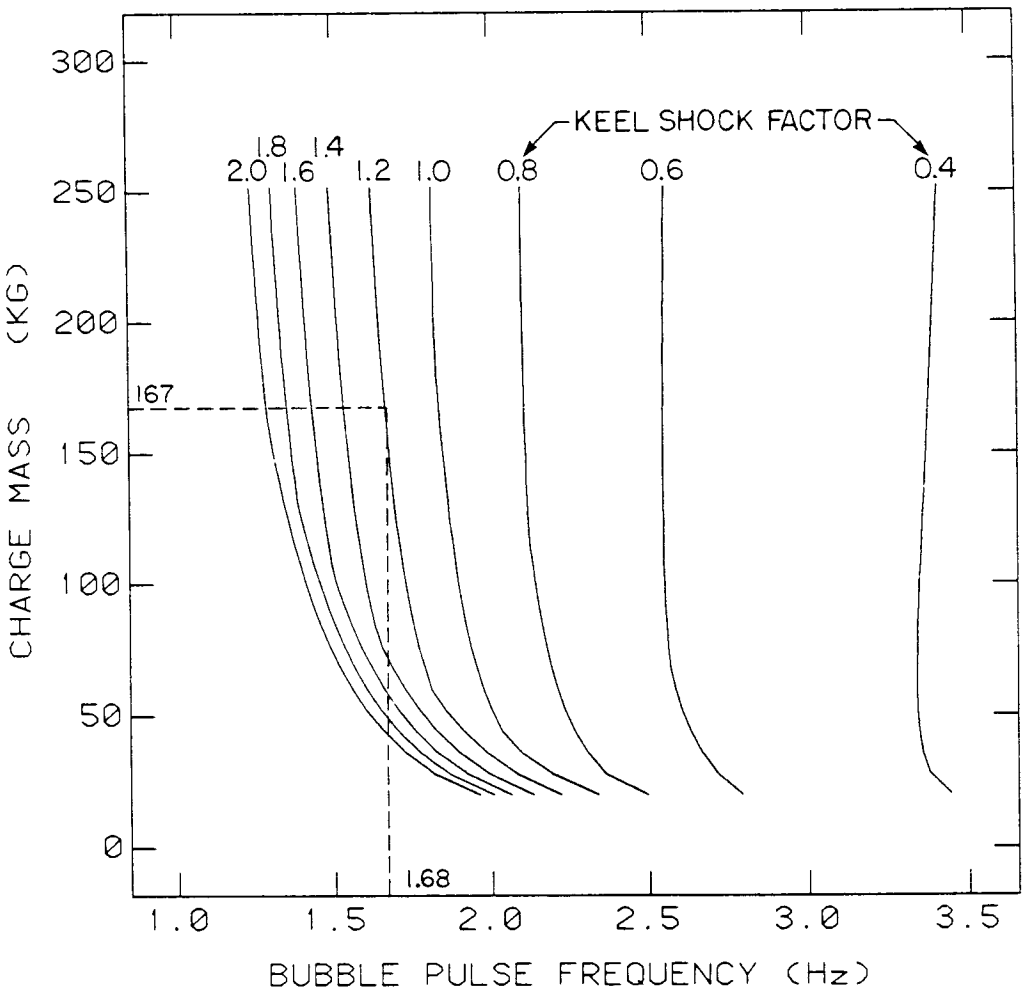

Figure 16: Charge mass versus bubble pulse frequency for various keel shock factors.

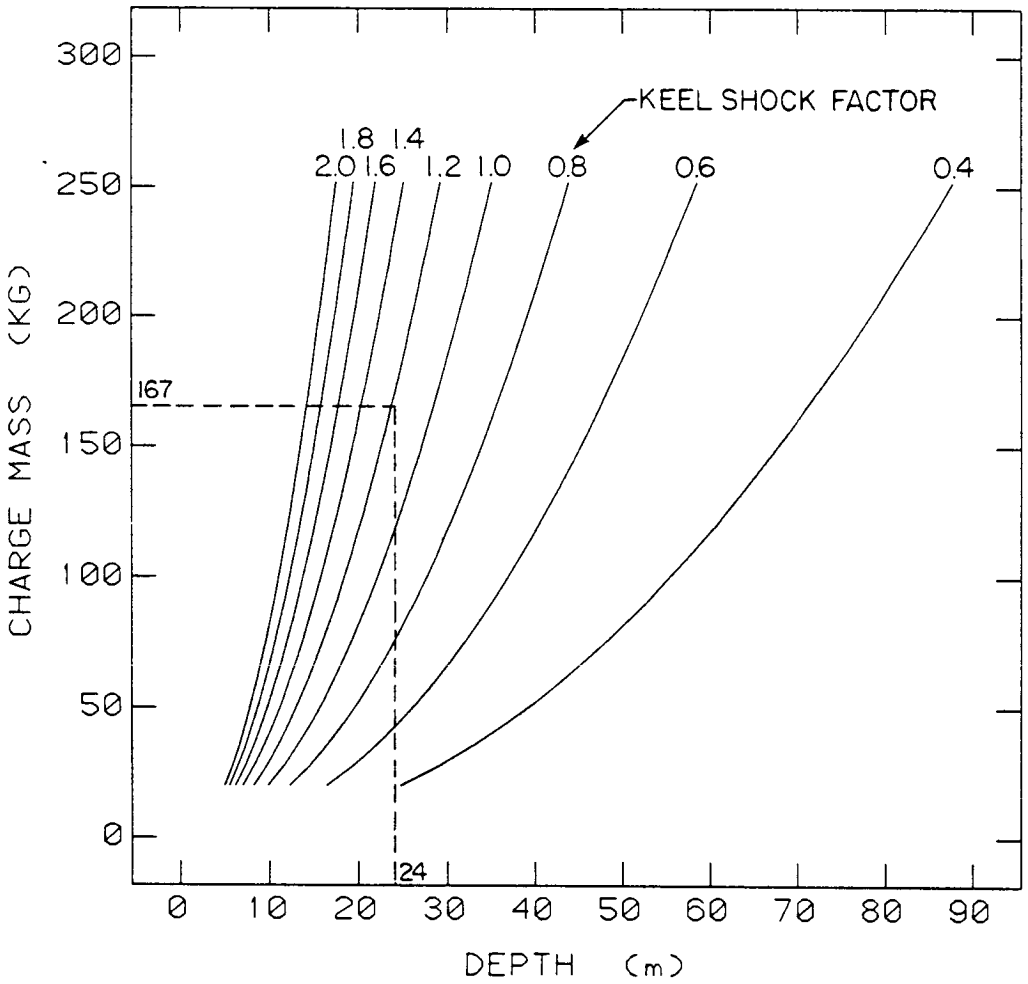

Figure 17: Charge mass versus depth for various keel shock factors.

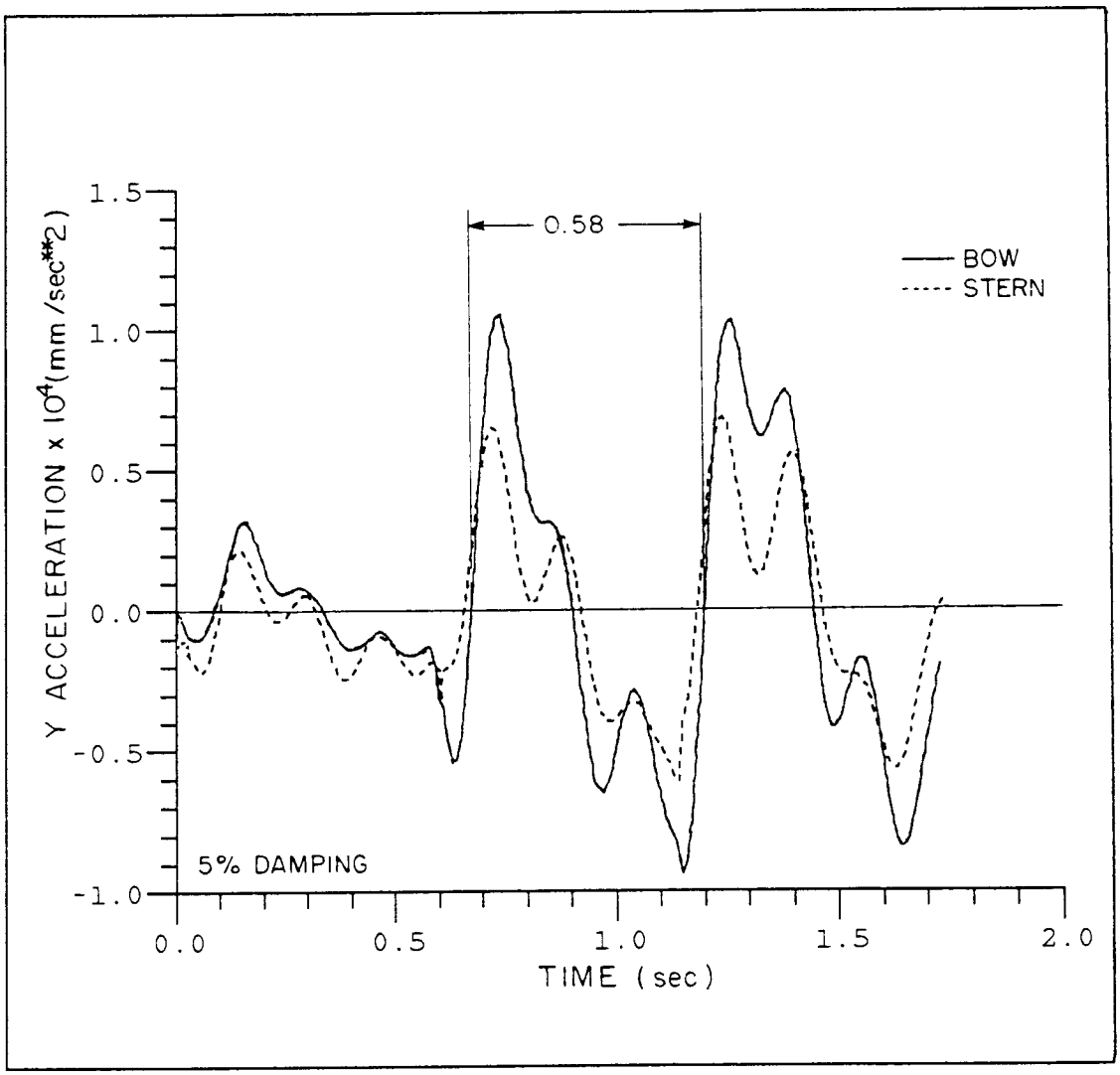

Figure 18: Acceleration response of the bow and stern of the test ship to a tuned bubble pulse loading (keel shock factor 1.19).

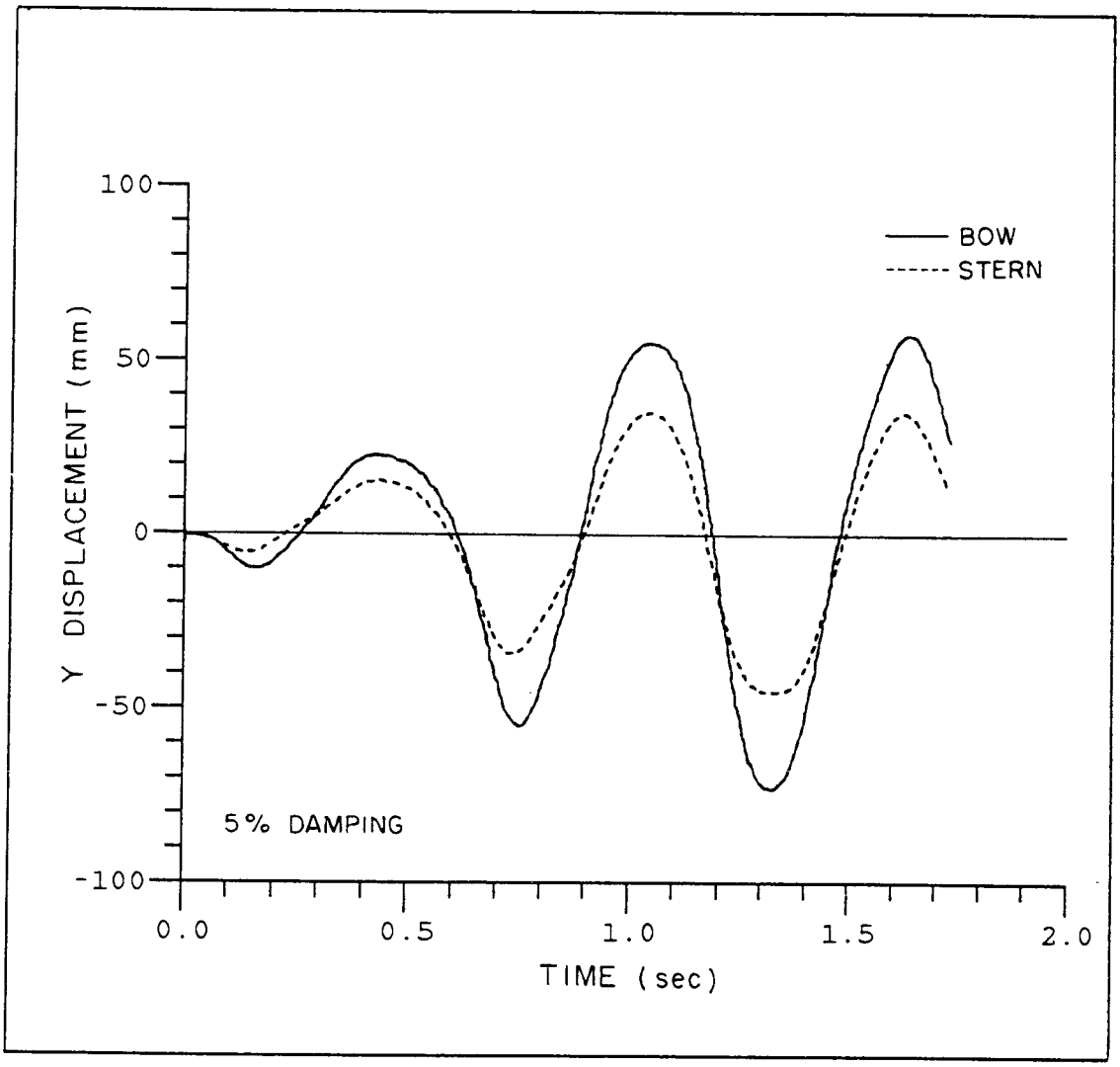

Figure 19: Displacement response of the bow and stern of the test ship to a tuned bubble pulse loading (keel shock factor 1.19).

Appendix - A sample run of the UBLOAD program

```
************************************************************
Sample run of the program UBLOAD. Program input is in lower
case for clarity.  *** indicates comments.
************************************************************

run ubload

ENTER THE 5 CHARACTER PREFIX OF THE EQ. BEAM FILE

ebcpf

FILES ARE TITLED ebcpf.TOT AND ebcpf.FRM


 UNITS ARE METERS,SECONDS,MEGAPASCALS


 NO. OF HYDROSTATIC SECTIONS AVAILABLE IS 20

 SCALE FACTOR IS 1.000000

 COMPUTING ADDED MASS VALUES....HANG ON

*** Program has located the required prefx.tot and prefx.frm
*** files. Bouyancy and fluid added mass terms are being
*** calculated.

 ENTER THE DEPTH OF DISCHARGE (METERS)

24

 ENTER PERPENDICULAR STANDOFF FROM THE SHIP CENTERPLANE

0

*** A value of zero indicates charge is directly under keel
```

```
 ENTER DISTANCE FROM FORWARD PERPENDICULAR TO THE
 STANDOFF PERPENDICULAR - NEGATIVE IF LOCATION
 FORWARD OF THE BOW

70

ENTER: 1 - FOR SPECIFICATION OF KEEL SHOCK FACTOR
       2 - FOR SPECIFICATION OF CHARGE MASS (KG TNT)
2


 ENTER CHARGE MASS IN KG OF TNT
167


 KEEL SHOCK FACTOR IS 1.189979


 BUBBLE MIGRATION TO BE INCLUDED? (Y=1,N=0)
1


 FREE SURFACE EFFECTS TO BE INCLUDED?(Y=1,N=0)
1

*** If migration and free surface effects are neglected, the
*** Tchebycheff method is offered as an option

 ENTER DRAG COEFFICIENT CD (0 FOR DEFAULT)
2.25

*** A default value of 2.25 is used in the program

 PULSE NO. 1
 LSCALE     TSCALE     DELTA     ZINIT
6.207467, 0.4162805, 1.610963, 5.477274
 ROOTS ARE 0.1012467, 0.9339422
 BUBBLE COEFFICIENT K IS 0.1793994
```

```
 PULSE NO. 2
 LSCALE     TSCALE     DELTA      ZINIT
5.293119, 0.3549632, 1.889245, 6.423434
 ROOTS ARE 0.2247397, 0.8706292
 BUBBLE COEFFICIENT K IS 0.3260855

 K VALUE EXCEEDS MAXIMUM FOR WHICH ROOTS ARE
 AVAILABLE ON PULSE 3. NO. OF PULSES LIMITED
 TO 2 FOR THIS EXPLOSION

*** See Section 2 of the report for a discussion of the k value.
*** Note that the value increases from pulse to pulse. The roots
*** correspond to the minimum and maximum radii predicted by the
*** deep bubble approximation formula. The minimum is used as the
*** initial condition for the integration. The scale factors, non-
*** dimensional depth (DELTA), and non-dimensional initial head
*** (ZINIT) parameters are printed for reference only.

 CONTINUE? (Y=1,N=0)
1

ENTER 8 CHARACTER FILENAME FOR STORAGE OF BUBBLE CHARACTERISTICS

D FOR DEFAULT

data.out


 ENTER INTEGRATION CUTOFF TIME IN SECONDS
 ZERO FOR DEFAULT VALUE
3.0

*** Typically no longer than 2.0-3.0 seconds required.
*** The default will give 4*TSCALE, or almost 3 bubble periods

 PULSE TRANSITION AT TIME STEP 113

*** Transition points are points of minimum radii.
```

```
*** Energy reduction is applied at those points if required.

BUBBLE TIME HISTORY CHARACTERISTICS WRITTEN ON  FILE data.out


ENTER: 1 - TO CREATE THE VAST .LOD FILE
       2 - TO OUPUT LOAD TIME HISTORY DATA
       3 - TO OUTPUT PRESSURE TIME HISTORY DATA
       4 - RESTART
       5 - STOP

NOTE: ALL FURTHER OUTPUT IS WRITTEN TO FILE ebcpf.LOD


 WRITING LOAD FILE...

ENTER: 1 - TO RESTART ANALYSIS
       2 - TO OBTAIN OTHER DATA FOR THIS RUN
       3 - TO STOP

3
CPU time 3.12   Elapsed time 1:51.85
```

References

1. Cole, R. H., Underwater Explosions, Princeton University Press, Princeton, N.J., 1948.

2. Chertok, G. W., 'The Flexural Response of a Submerged Solid to a Pulsating Gas Bubble', J. of Applied Physics, Vol. 24, No. 2, 1953, pp. 192-197.

3. Herring, C. 'Theory of the Pulsations of the Gas Bubble Produced by an Underwater Explosion', Underwater Explosion Research, Vol. 2, The Gas Globe, Office of Naval Research, 1950.

4. Heaton, K., 'The Effect of Non-sphericity on the Migration of the Gas Bubble from Underwater Explosions', DREV Report, Annex to AC/141(IEG/6)SG/7-WP/24, Quebec, 1985.

5. Hicks, A. N., 'The Theory of Explosion Induced Ship Whipping Motions', NCRE Report R579, 1972.

6. Wilkerson, S. A. 'Elastic Whipping Response of Ships to an Underwater Explosion Loading', MScE Thesis, George Washington University, 1985.

7. Bannister, K. A., 'Whipping Techniques for Ships and Submarines', Part 3, Shock and Vibration Bulletin, NRL Washington, D.C., September, 1980.

8. Vernon, T. A., Painchaud, G., DREA informal communication

9. Lewis, F. M., 'The Inertia of Water Surrounding a Vibrating Ship', Transactions SNAME, Vol. 37, 1929.

10. Arons, A. B., 'Secondary Pressure Pulses Due to Gas Globe Oscillation in Underwater Explosions, and Selection of Adiabatic Parameters in the Theory of Oscillation', Underwater Explosion Res. Vol. 2, The Gas Globe, Office of Naval Research, 1950.

11. Abramowitz, M., Stegun, I., Handbook of Mathematical Functions, Dover Publications, New York, 1970.

12. Vernon, T. A., 'SCRAP - A Computer Program for Elastic Strength Analysis and Equivalent Beam Modelling of Ship Hulls', DREA TM 86/214, 1986.

13. 'Vibration and Strength Analysis Program VAST04', DREA contract reports, Martec Ltd., 1986.

14. 'Structural Design of Surface Warships', DMEM-10 Part IV, Canadian Department of National Defence, 1982.

Unclassified
Security Classification

DOCUMENT CONTROL DATA – R & D
(Security classification of title, body of abstract and indexing annotation must be entered when the overall document is classified)

1. ORIGINATING ACTIVITY Defence Research Establishment Atlantic	2a. DOCUMENT SECURITY CLASSIFICATION Unclassified 2b. GROUP

3. DOCUMENT TITLE
WHIPPING RESPONSE OF SHIP HULLS FROM UNDERWATER EXPLOSION BUBBLE LOADING

4. DESCRIPTIVE NOTES (Type of report and inclusive dates) Technical Memorandum

5. AUTHOR(S) (Last name, first name, middle initial)
Vernon, Thomas, A.

6. DOCUMENT DATE December 1986	7a. TOTAL NO. OF PAGES 47	7b. NO. OF REFS 14
8a. PROJECT OR GRANT NO.	9a. ORIGINATOR'S DOCUMENT NUMBER(S) DREA TECHNICAL MEMORANDUM 86/225	
8b. CONTRACT NO.	9b. OTHER DOCUMENT NO.(S) (Any other numbers that may be assigned this document)	

10. DISTRIBUTION STATEMENT
Qualified requesters may obtain copies of this document from their defence documentation center.

11. SUPPLEMENTARY NOTES	12. SPONSORING ACTIVITY

13. ABSTRACT

S// A summary of the bubble pulsation dynamics of an underwater explosion is presented with the aim of establishing the whipping response of a nearby surface ship. The effects of the initial shock front are not considered and the fluid is assumed to be an incompressible medium. The gas bubble volume dynamics can then be related to far field fluid accelerations assuming that a potential flow condition is satisfied. Given the effective mass of the ship comprising the added fluid and buoyancy mass contributions, the forces on the ship resulting from the accelerated flow field can be determined. The theory considers the effects of proximity of the explosion bubble to a free surface, vertical migration of the bubble due to the hydrostatic imbalance, and an energy dissipative mechanism introduced via a pseudo pressure drag coefficient. The theory is applied in analyses of the whipping displacements and stresses induced in the hull of a typical frigate-size warship subjected to underwater blast loading. The response is obtained using a modal superposition of the wet hull modes of a detailed equivalent beam model of the hull. //

DSIS
78-070

D R E A

C R D A